IET Radar, Sonar & Navigation

Research Article

IET Journals
The Institution of Engineering and Technology

Experimental validation of coherent multiple-input multiple-output radar antenna patterns

ISSN 1751-8784
Received on 10th April 2015
Revised on 29th June 2015
Accepted on 30th June 2015
doi: 10.1049/iet-rsn.2015.0196
www.ietdl.org

Peter W. Moo ✉, *Pascale Sévigny*, *Tony Laneve*

Radar Sensing and Exploitation Section, Defence Research and Development Canada, Ottawa, Canada K1A 0Z4
✉ *E-mail: Peter.Moo@drdc-rddc.gc.ca*

Abstract: This study specifies the antenna radiation patterns of a linear array radar operating in a phased array configuration and in two colocated multiple-input multiple-output (MIMO) configurations. The MIMO-1 configuration uses orthogonal transmission on all elements, while the MIMO-2 configuration uses orthogonal transmission on the two end elements. The theoretical two-way antenna radiation patterns are derived for all three configurations. Field experiments with an eight-element, *X*-band linear array radar and trihedral targets are then described. The experimental mainbeam patterns are shown to match those of the theoretical patterns. MIMO-1 is shown to have the same two-way radiation pattern as that of the phased array radar configuration. Compared with MIMO-1 and phased array, MIMO-2 has enhanced angle estimation accuracy, lower gain, and higher sidelobes while only requiring two orthogonal waveforms on transmit.

1 Introduction

A linear array radar is traditionally operated as a phased array radar, where a single waveform is transmitted coherently on the array. Recently, there has been increasing interest in multiple-input, multiple-output (MIMO) radar, which uses multiple transmitters and multiple receivers [1–4]. MIMO operation requires the use of orthogonal waveforms on transmit and increased signal processing on receive, and therefore has increased complexity and flexibility compared with the phased array operation. In this work, attention is focused on coherent MIMO radar, where the transmitters and receivers are co-located. The coherent MIMO radar has a number of potential benefits, including the use of omnidirectional search modes [5], enhanced clutter cancellation [6], and increased Doppler resolution [7].

Owing to the increased complexity of MIMO radar, it is important to gain an accurate understanding of its potential benefits. In particular, it has been previously stated that MIMO radar has enhanced angle estimation accuracy compared with the phased array radar. This increased accuracy results from an apparent decrease in antenna beamwidth when the linear array is operated as an MIMO radar [8–12]. However, it is not necessarily clear from the previous work whether the antenna radiation patterns under consideration are one- or two-way patterns. The configuration of transmitters and receivers also plays a role in determining the antenna radiation patterns, and therefore the angle estimation accuracy, of MIMO radar [10]. The effect of transmitter and receiver configuration on antenna radiation patterns has not been fully explored.

This paper compares the antenna beamwidth of a linear array radar that is operated in phased array and MIMO configurations. The theoretical two-way antenna patterns are derived for phased array radar and two MIMO radar configurations. This paper then describes a MIMO radar testbed, as well as field experiments conducted with the testbed, laboratory equipment, and trihedral targets. The measured antenna beamwidths from field experimental data are shown to verify the theoretical antenna beamwidths. These theoretical and experimental antenna beamwidth results specify the angle estimation accuracy of a coherent MIMO radar.

2 Theoretical antenna patterns

Two-way antenna radiation patterns are derived for an N-element linear array operating in three distinct configurations: phased array, MIMO-1, and MIMO-2. In the phased array configuration, a single waveform is transmitted coherently across the array, and the return is received coherently on all elements. For the MIMO-1 configuration, each element transmits a distinct orthogonal waveform, and the return is received coherently on all elements. For the MIMO-2 configuration, each of the end elements transmits a distinct orthogonal waveform, and the return is received coherently on the first N–1 elements. The MIMO-2 configuration is a special case of $M \times N$ spatial multiplexing MIMO [10]. See Fig. 1 for an illustration of the configurations. Each element in the array has element pattern $E(\theta)$, where θ is the azimuth angle. A linear array with N elements has an array factor $A_N(\theta)$, given by

$$A_N(\theta) = \frac{\sin^2 [N\pi(d/\lambda)\sin\theta]}{N^2 \sin^2 [\pi(d/\lambda)\sin\theta]},$$

where d is the inter-element spacing and λ is the wavelength.

For the phased array configuration, the transmit radiation pattern $G_{\mathrm{PA,Tx}}(\theta)$ and the receive radiation pattern $G_{\mathrm{PA,Rx}}(\theta)$ are equal, so that $G_{\mathrm{PA,Tx}}(\theta) = G_{\mathrm{PA,Rx}}(\theta) = E(\theta)A_N(\theta)$ [13]. The phased array two-way radiation pattern $G_{\mathrm{PA,2\text{-}way}}(\theta)$ is given by

$$\begin{aligned} G_{\mathrm{PA,2-way}}(\theta) &= G_{\mathrm{PA,Tx}}(\theta)G_{\mathrm{PA,Rx}}(\theta) \\ &= E(\theta)^2 A_N(\theta)^2. \end{aligned} \quad (1)$$

For the MIMO-1 configuration, the transmit radiation pattern $G_{\mathrm{M1,Tx}}(\theta)$ is given by the element pattern, $G_{\mathrm{M1,Tx}}(\theta) = E(\theta)$. On receive, the effective array is the spatial convolution of the transmit linear array and the receive linear array [10]. Therefore, the MIMO-1 receive array factor is the product of an N-element linear array factor by itself, that is, $A_N(\theta)^2$. The MIMO-1 receive radiation pattern $G_{\mathrm{M1,Rx}}(\theta)$ is then specified by $G_{\mathrm{M1,Rx}}(\theta) = E(\theta)A_N(\theta)^2$. The MIMO-1 two-way radiation pattern

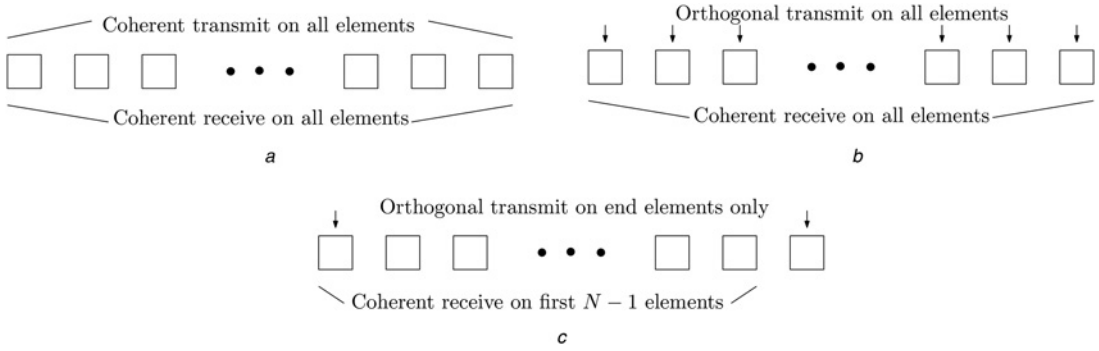

Fig. 1 *Configurations for an N-element linear array radar*

a Phased array
b MIMO-1
c MIMO-2

$G_{\mathrm{M1,2\ -way}}(\theta)$ is given by

$$G_{\mathrm{M1,2-way}}(\theta) = G_{\mathrm{M1,Tx}}(\theta)G_{\mathrm{M1,Rx}}(\theta) = E(\theta)^2 A_N(\theta)^2. \tag{2}$$

The two-way radiation pattern for the MIMO-1 configuration is equal to the two-way radiation pattern for the phased array configuration.

For the MIMO-2 configuration, the transmit radiation pattern $G_{\mathrm{M2,Tx}}(\theta)$ is given by the element pattern, $G_{\mathrm{M2,Tx}}(\theta) = E(\theta)$. On receive, the effective array is the spatial convolution of the transmit linear array and the receive linear array. Therefore, the MIMO-2 receive array factor is that of a linear array with $2N-2$ elements. The MIMO-2 receive radiation pattern $G_{\mathrm{M2,Rx}}(\theta)$ is then specified by $G_{\mathrm{M2,Rx}}(\theta) = E(\theta)A_{2N-2}(\theta)$. The MIMO-2 two-way radiation pattern $G_{\mathrm{M2,2\ -way}}(\theta)$ is given by

$$G_{\mathrm{M2,2-way}}(\theta) = G_{\mathrm{M2,Tx}}(\theta)G_{\mathrm{M2,Rx}}(\theta) = E(\theta)^2 A_{2N-2}(\theta). \tag{3}$$

Equivalent radiation patterns can be derived using the formulation from [3, Ch. 4], as follows. For $i = 1, \ldots, N$, element i transmits a bandpass signal $s_i(t)\mathrm{e}^{\mathrm{j}\omega t}$, where $s_i(t)$ is the transmitted baseband complex envelope and ω is the carrier angular frequency. The vector $\boldsymbol{s}(t)$ is given by

$$\boldsymbol{s}(t) = [s_1(t), \ \ldots, s_N(t)]^{\mathrm{T}},$$

where $(\cdot)^{\mathrm{T}}$ denotes the transpose. The N-element steering vector is given by

$$\boldsymbol{a}_N(\theta) = [\mathrm{e}^{-\mathrm{j}\omega\tau_1(\theta)}, \ \ldots, \mathrm{e}^{-\mathrm{j}\omega\tau_N(\theta)}],$$

where $\tau_i(\theta)$ is the propagation delay of element i relative to the first element along the direction θ. The transmit signal correlation matrix is given by

$$\boldsymbol{R}_S = \int_{T_0} \boldsymbol{s}(t)\boldsymbol{s}^{\mathrm{H}}(t)\mathrm{d}t,$$

where T_0 is the time extent of the transmitted baseband complex envelopes and $(\cdot)^{\mathrm{H}}$ denotes the Hermitian operation.

As derived in [3, Ch. 4], the phased array configuration has the signal correlation matrix $\boldsymbol{R}_S = \boldsymbol{a}_N^*(\theta_0)\boldsymbol{a}_N^{\mathrm{T}}(\theta_0)$, where $(\cdot)^*$ denotes conjugate transpose and the transmit signal is steered to angle θ_0. The phased array transmit–receive pattern is given by

$$\Gamma_{\mathrm{PA}}(\theta, \theta_d) = C\frac{\left|\boldsymbol{a}_N^{\mathrm{H}}(\theta)\boldsymbol{a}_N(\theta_d)\right|^2 \cdot \left|\boldsymbol{a}_N^{\mathrm{H}}(\theta)\boldsymbol{a}_N(\theta_0)\right|^2}{N}, \tag{4}$$

where C is a normalisation constant and the receive beam is steered to θ_d.

For the MIMO-1 configuration, the transmit signal correlation matrix is the N-dimensional identity matrix, $\boldsymbol{R}_S = I_N$, so that the MIMO-1 transmit–receive pattern is given by

$$\Gamma_{\mathrm{M1}}(\theta, \theta_d) = C\frac{\left|\boldsymbol{a}_N^{\mathrm{H}}(\theta)\boldsymbol{a}_N(\theta_d)\right|^4}{N^2}. \tag{5}$$

For the MIMO-2 configuration, the transmit signal correlation matrix has (i, j) entries given by

$$\boldsymbol{R}_S(i,j) = \begin{cases} 1 & \text{if } i = j = 1 \quad \text{or} \quad i = j = N \\ 0 & \text{otherwise} \end{cases}$$

The MIMO-2 transmit–receive pattern is given by (see eq. (6) at the bottom of the next page)

where the right-hand side of (6) is equivalent to the phased array transmit–receive pattern for a linear array with 2N–2 elements.

3 Description of MIMO radar experiments

3.1 The experimental setup

A time-division coherent MIMO radar was operated on an open field with a 75 cm side trihedral as a target, positioned at 45 m range from the MIMO array, 4.6° off boresight in azimuth, and a height of ∼1.0 m. For a different scene, the target was positioned at 45 m range from the MIMO array, 14.8° off boresight in azimuth, and a height of ∼1.6 m. A 45 cm side trihedral was used as a calibration target, and positioned at 35 m range, −4.8° off boresight in azimuth, and a height of ∼1.7 m. The experimental setup is shown in the right photograph of Fig. 2. The ground truth for this experiment was obtained using a Leica total station TS15.

$$\Gamma_{\mathrm{M2}}(\theta, \theta_d) = C\frac{\left|\boldsymbol{a}_{N-1}^{\mathrm{H}}(\theta)\boldsymbol{a}_{N-1}(\theta_d)\right|^2 \cdot \left(\left[\mathrm{e}^{-\mathrm{j}\omega\tau_1(\theta)}\mathrm{e}^{-\mathrm{j}\omega\tau_1(\theta_d)}\right]^2 + \left[\mathrm{e}^{-\mathrm{j}\omega\tau_N(\theta)}\mathrm{e}^{-\mathrm{j}\omega\tau_N(\theta_d)}\right]^2\right)}{2(N-1)}, \tag{6}$$

IET Radar Sonar Navig., 2016, Vol. 10, Iss. 2, pp. 341–347

Fig. 2 *Photographs of the linear array (left) and the setup (right) for the time-division coherent MIMO experiment*

3.2 The array

The MIMO linear array was assembled out of ten Narda 640 horn antennae [14], as shown on the left photograph of Fig. 2. The array was mounted on a tripod ~ 2.35 m above the ground. The eight central elements of the array were active while the two end elements were terminated. The antenna elements were positioned 8.2 cm apart and were operated at 9 GHz. At this frequency, grating lobes are expected every 24°. The dimensions of the Narda 640 horn antennae are 5.954 cm × 7.859 cm, and their beamwidths are estimated to be 30° and 32° at 9 GHz, in the *E* and the *H* planes, respectively. For this experiment, vertical polarisation was used.

3.3 MIMO radar data collection

Fig. 3 shows the schematic diagram of a time-division eight-channel MIMO radar testbed. An arbitrary waveform generator (AWG1) produced differential *I/Q* signals, which were routed to the wideband input ports of a vector signal generator, (VSG1). The VSG upconverted the base-band *I/Q* signal to *X*-band. This resulted in a linear frequency modulated (LFM) signal centred at 9.0 GHz, with a bandwidth of 150 MHz, and a pulse width of 100 μs. The chirp rate was 1.5 MHz/μs. The transmit signal was routed sequentially to each of the eight transmit/receive antennas via a SP10T microwave switch, SW1. The received signal was routed via SP2T switches, SW2–SW5, to the four channels of a digital oscilloscope, OSC1. The measurement was fully automated and used Agilent's Signal Studio for Pulse Building (SSPB), N7620B, to generate the transmit waveform, and Agilent's Vector Signal Analysis (VSA) software to demodulate, decimate, and perform data transfer of the digitised time-domain data. The control of the SSPB and VSA software along with switch control and data storage was accomplished via in-house code written in Agilent's VeePro 9.3 software. The VeePro software interfaces with the SSPB and VSA software packages via .COM and .NET APIs, respectively.

Prior to measurement, a calibration was performed in order to flatten the frequency response of the transmit signal. The spectrum analyser, SA1, was connected to the ends of each of the RF cables (CAB1-8) in turn. The AWG and VSG produced a CW tone which was swept across a frequency band centred at 9.0 GHz with a bandwidth of 250 MHz. The SSPB software then used this information to predistort the base band *I/Q* signals such that a flat frequency response was obtained at the antenna input. The calibrated signals for each of the eight paths of the transmit signal were stored and applied during the measurement. During the calibration, the power at the antenna input was measured and adjusted such that it was equal for all the eight channels.

The measurement procedure involved transmitting a signal on one transmit channel, then receiving it on the four odd numbered receive channels simultaneously (i.e. receive channels Rx1, Rx3, Rx5, and Rx7). The transmit switch, SW1, was then switched to the next transmit channel and the signal was received on the same four odd numbered receive channels. This procedure was repeated until the transmit signal had been transmitted through all eight transmit channels. The receive switches, SW2–SW5, were then toggled such that the even numbered receive channels, Rx2, Rx4, Rx6, and Rx8, were now connected to OSC1 and the odd numbered receive channels were terminated into 50 Ω. The transmit signal was now transmitted in sequence through each transmit channel (via SW1) and received on the four even numbered receive channels simultaneously.

When the measurement procedure was completed, data for a complete 8 × 8 time-division MIMO system was obtained. The data was stored in Matlab compatible .mat files.

The signal processing algorithms consisted of pulse compression, array calibration, and MIMO beamforming. De-chirping of the 64 received signals was performed by complex multiplication with the complex conjugate of the transmitted waveform. A fast Fourier transform then provided a pulse compressed range profile for each of the 64 channels. Array calibration was performed by using the 64 range profiles and the known positions of the antenna array elements and of the calibration target located at 35 m range. For each transmit–receive element pair, the delay and phase due to propagation from the transmit element to the calibration target and back to the receive element were determined. The corresponding range profile was then shifted in range. This was a coarse correction for cable lengths and various delays introduced by the equipment. A finer correction was then applied as a phase correction. This process was repeated for all combinations of transmit and receive channels, producing 64 calibrated range profiles. MIMO beamforming was performed using the following delay-and-sum method [15]. The two-way distance and phase due to propagation from transmit antenna *A* to a given point in space and back to receive element *B* was determined. The two-way distances and phases for all combinations of transmit and receive elements were determined. The two-way distances were used to select the signals from the appropriate range bins in the calibrated range profiles. The phases were used to compensate the received signals. For beamforming using the MIMO-1 configuration, the resulting 64-phase compensated complex signals corresponding to the point in space were summed. For beamforming using any other MIMO configuration such as MIMO-2, the appropriate subset of the 64-phase compensated complex signals were summed. This process was repeated for all points in the space of interest.

3.4 Phased array radar data collection

To mimic a phased array data collection, a mixed experiments and simulations approach (MESA) was developed. The objective was to measure the impulse response of the system composed of the antenna array and scene being viewed including the targets. It is assumed that the system is linear and that there is no change in the impulse response over the time taken to perform the measurement. A 16-port vector network analyser (VNA) was connected via appropriate cabling to each port of the antenna array. Multi-port calibration of the VNA was performed using an electronic calibration module. The reference plane for the measurement was established at the VNA output ports. The 8-port *S*-parameters of the scene were measured over a broad bandwidth (from 10 MHz to 18 GHz) with sufficient frequency resolution to ensure proper

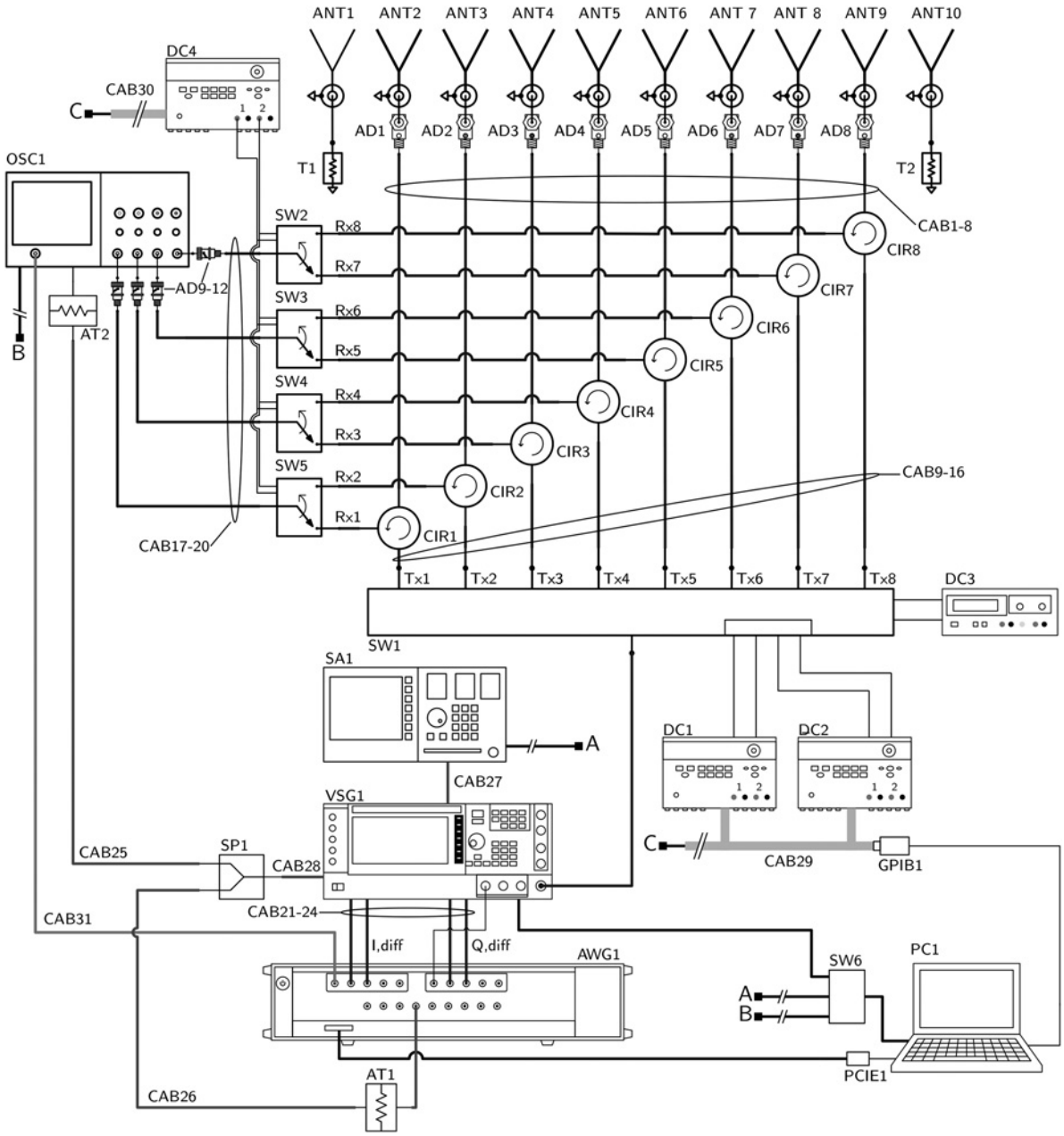

Fig. 3 *Schematic diagram of the time-division MIMO radar testbed*

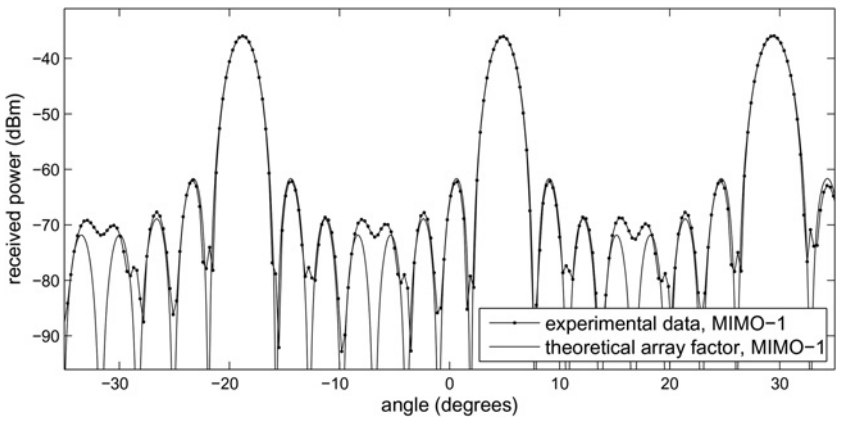

Fig. 4 *Azimuth profile for a scene with one target located at 4.6°. The theoretical array pattern, scaled and steered in azimuth, is shown for comparison*

IET Radar Sonar Navig., 2016, Vol. 10, Iss. 2, pp. 341–347

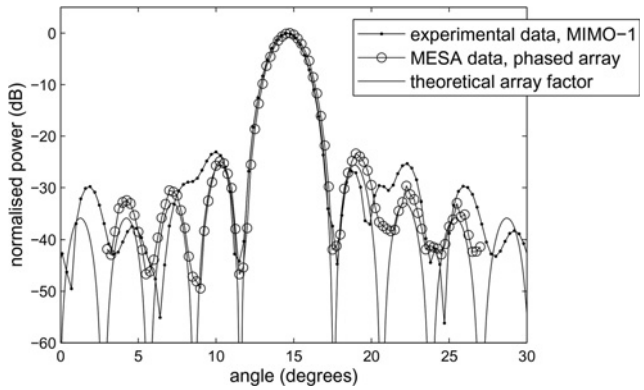

Fig. 5 *Azimuth profile for a scene with one target located at 14.8° for the MIMO-1 experimental data and MESA phased array data. The theoretical array pattern, scaled and steered in azimuth, is shown for comparison*

phase sampling at distances where the targets were located. The resulting *S*-parameter file was imported into the Agilent ADS Electronic Design and Automation software package for analysis. A transient/convolution simulation was then performed using an ideal LFM signal source at a centre frequency of 9 GHz to stimulate the 8-port network. Appropriate delay values were added to each antenna port such that the array was steered over the desired azimuth angle. The return signals from each antenna were combined to produce the final output. The signal was then pulse compressed and transformed into the frequency domain. The peak value was plotted versus angle as shown in Fig. 5.

4 Results

In this section, the theoretical radiation patterns from Section 2 are compared with the data processing results of the experiments described in Section 3. Since the element pattern components of (1)–(3) are identical, the array factor components are compared.

Fig. 4 shows the experimental data collected with one target located at 4.6° and beamformed with a MIMO-1 configuration. The theoretical array pattern $A_N(\theta)^2$ is shown for comparison. The array pattern is scaled in amplitude to match the experimental data and steered in azimuth towards the target location. The experimental data matches the theoretical array pattern, including the grating lobes. The main beam location is in agreement with the ground truth data.

The two-way phased array and MIMO-1 array factors are now compared in Fig. 5 for experimental data collected using the MESA and the time-division MIMO radar, respectively, for the scene with one target located at 14.8°. The experimental two-way phased array and MIMO-1 array factors are identical for the main beam location and width, and are in agreement with (1) and (2). The higher sidelobes of the experimental MIMO-1 data are due to experimental data collection conditions that is lower dynamic range and larger amount of jitter.

Fig. 6 shows the experimental data collected with one target located at 4.6°, processed for both MIMO-1 and MIMO-2 configurations. On the top graph, the azimuth profiles are shown as normalised values. We can clearly see the improved resolution of the MIMO-2 array over the MIMO-1 array, at the expense of larger sidelobes (13 versus 26 dB main-to-first sidelobe ratio for the MIMO-2 and MIMO-1 arrays, respectively). On the bottom graph, the azimuth profiles are shown without normalisation and we see a gain loss of ~13 dB for MIMO-2 array.

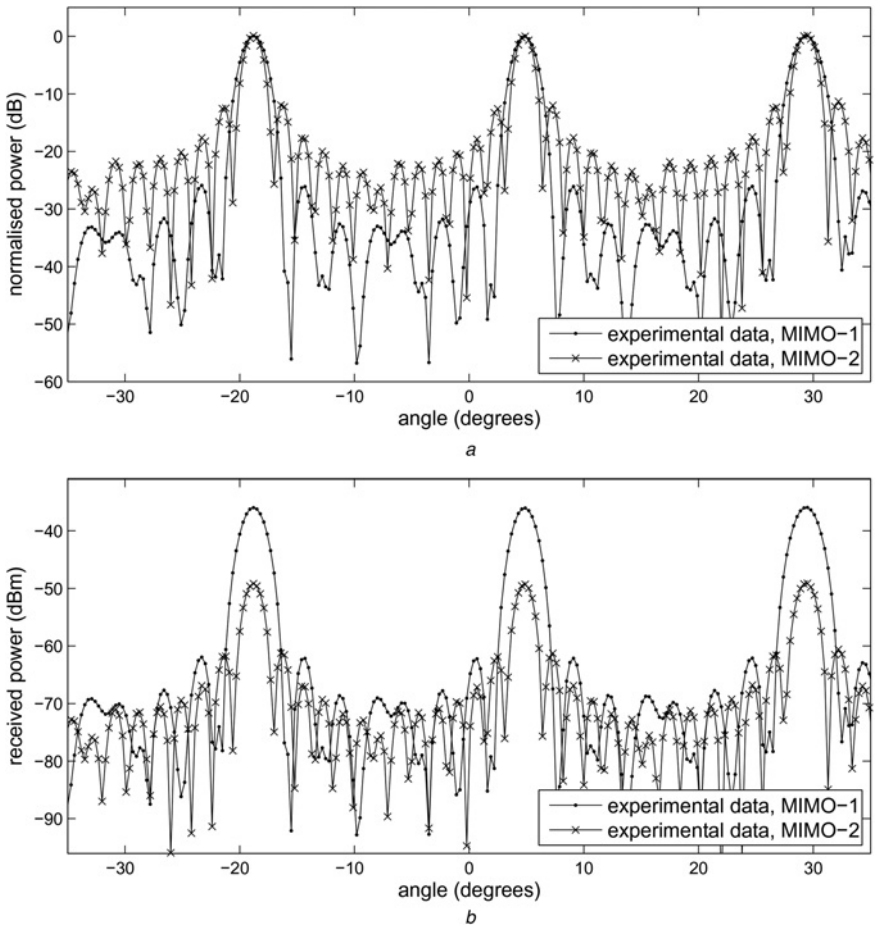

Fig. 6 *Azimuth profiles for scene 2 with one target located at 4.6°, processed for MIMO-1 and MIMO-2 configurations*

a Normalised power values
b Received power values

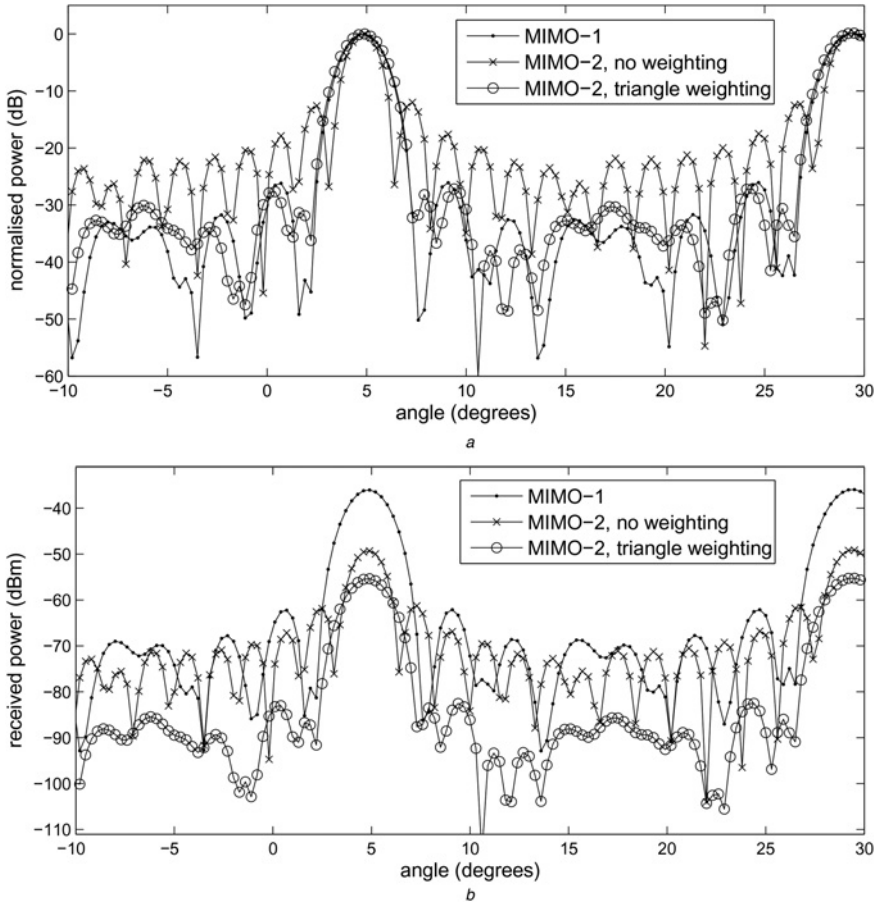

Fig. 7 *Azimuth profiles for one target located at 4.6°, processed for MIMO-1 and MIMO-2 experimental data with and without triangle weighting*

a Normalised power values
b Received power values

Indeed, given that our MIMO beamforming algorithms are based on a sum, without scaling, the received power is expected to scale as

$$10\log_{10}(N_{\mathrm{Tx}}N_{\mathrm{Rx}})^2, \tag{7}$$

where N_{Tx} and N_{Rx} are the number of transmit and receive elements, respectively.

The higher sidelobes can be circumvented by using appropriate weighting of the MIMO channels before summation. In fact, the MIMO-1 configuration can be viewed as a triangle weighting of the MIMO-2 configuration. The convolution of the transmit and the receive arrays, that is the virtual array, is the convolution of two rectangle functions for the MIMO-1 configuration and results in a triangle with coefficients [1,2,3,4,5,6,7,8,7,6,5,4,3,2,1]/8. The virtual array of the MIMO-2 configuration is an array of 14 elements each with a coefficient of 1. In Fig. 7, we have reproduced the results of Fig. 6 for the MIMO-1 and MIMO-2 arrays. We also have plotted the results for MIMO-2 array using a triangle weighting with coefficients [1,2,3,4,5,6,7,7,6,5,4,3,2,1]/8 to mimic as closely as possible the MIMO-1 array. The results show that using this weighting we can recover the results of MIMO-1 in terms of beamwidth and sidelobes, with much reduced complexity, at the expense of further gain loss.

5 Conclusions

For a linear array radar, it has been shown that the phased array and MIMO-1 configurations have identical theoretical antenna patterns, while the MIMO-2 configuration has an antenna pattern with narrower mainbeam beamwidth but higher sidelobes. Measured beamwidths from field experimental data verified the theoretical beamwidths. In comparing the MIMO-1 and MIMO-2 configurations, MIMO-2 has a narrower beamwidth and therefore enhanced angle estimation accuracy, at the expense of lower gain and higher sidelobes. MIMO-2 requires only two orthogonal waveforms on transmit, which simplifies waveform design [16, 17] and reduces the range–Doppler migration that results from longer integration times [18].

6 Acknowledgments

The authors thank Pietro Reitano for his contribution to the data collection, and Agilent for the lease of the VNA.

7 References

1 Melvin, W., Scheer, J.: 'Principles of modern radar: advanced techniques' (SciTech Publishing, 2012)
2 Gini, F., Maio, A.D., Patton, L.: 'Waveform design and diversity for advanced radar systems' (The Institution of Engineering and Technology, 2011)
3 Li, J., Stoica, P.: 'MIMO radar signal processing' (Wiley, 2009)
4 Davis, M., Showman, G., Lanterman, A.: 'Coherent MIMO radar: the phased array and orthogonal waveforms', *IEEE Aerosp. Electron. Syst. Mag.*, 2014, **29**, (8), pp. 76–91
5 Stoica, P., Li, J., Xie, Y.: 'On probing signal design for MIMO radar', *IEEE Trans. Signal Process.*, 2007, **55**, (8), pp. 4151–4161
6 Rabideau, D.: 'Non-adaptive multiple-input, multiple-output radar techniques for reducing clutter', *IET Radar Sonar Navig.*, 2009, **3**, (4), pp. 304–313
7 Forsythe, K., Bliss, D., Fawcett, G.S.: 'Multiple-input multiple-output (MIMO) radar: performance issues'. Conf. Record of the 38th Asilomar Conf. on Signals, Systems and Computers, 2004, 2004, vol. 1, pp. 310–315
8 Rabideau, D., Parker, P.: 'Ubiquitous MIMO multifunction digital array radar'. Conf. Record of the 37th Asilomar Conf. on Signals, Systems and Computers, 2003, vol. 1, pp. 1057–1064

9 Bekkerman, I., Tabrikian, J.: 'Target detection and localization using MIMO radars and sonars', *IEEE Trans. Signal Process.*, 2006, **54**, (10), pp. 3873–3883
10 Robey, F., Coutts, S., Weikle, D., *et al.*: 'MIMO radar theory and experimental results'. Conf. Record of the 38th Asilomar Conf. Signals, Systems and Computers, 2004, November 2004, vol. 1, pp. 300–304
11 Bliss, D., Forsythe, K.: 'Multiple-input multiple-output (MIMO) radar and imaging: degrees of freedom and resolution'. Conf. Record of the 37th Asilomar Conf. Signals, Systems and Computers, 2003, 2003, vol. 1, pp. 54–59
12 Forsythe, K., Bliss, D.: 'Waveform correlation and optimization issues for MIMO radar'. Conf. Record of the 39th Asilomar Conf. Signals, Systems and Computers, 2005, 2005, pp. 1306–1310
13 Eaves, J., Reedy, E.: 'Principles of modern radar' (Chapman and Hall, 1987)
14 English, E.K.: 'Measuring techniques for the calibration of standard gain horn antennas'. Technical Report ESL-711587-3, Ohio State University Colombus Electroscience Laboratory, 1980
15 Soumekh, M.: 'Synthetic aperture radar signal processing' (John Wiley and Sons, 1999)
16 Fuhrmann, D., San Antonio, G.: 'Transmit beamforming for MIMO radar systems using signal cross-correlation', *IEEE Trans. Aerosp. Electron. Syst.*, 2008, **44**, (1), pp. 171–186
17 Jindong, Z., Kerang, W., Xiaohua, Z.: 'Spatial-dependent waveform design for colocated uniform linear array multiple-input multiple-output radar', *IET Radar Sonar Navig.*, 2011, **5**, (5), pp. 545–550
18 Moo, P., Ding, Z.: 'Tracking performance of MIMO radar for accelerating targets', *IEEE Trans. Signal Process.*, 2013, **61**, (21), pp. 5205–5216